



Accepted Article

Title: An Ethacrynic Acid-Brominated BODIPY Photosensitizer (EA-BPS) Construct Enhances the Lethality of Reactive Oxygen Species in Hypoxic Tumor-Targeted Photodynamic Therapy

Authors: Jonathan L. Sessler, Miae Won, Seyoung Koo, Hao Li, Jin Yong Lee, Amit Sharma, and Jong Sung Kim

This manuscript has been accepted after peer review and appears as an Accepted Article online prior to editing, proofing, and formal publication of the final Version of Record (VoR). This work is currently citable by using the Digital Object Identifier (DOI) given below. The VoR will be published online in Early View as soon as possible and may be different to this Accepted Article as a result of editing. Readers should obtain the VoR from the journal website shown below when it is published to ensure accuracy of information. The authors are responsible for the content of this Accepted Article.

To be cited as: *Angew. Chem. Int. Ed.* 10.1002/anie.202012687

Link to VoR: <https://doi.org/10.1002/anie.202012687>

RESEARCH ARTICLE

An Ethacrynic Acid-Brominated BODIPY Photosensitizer (EA-BPS) Construct Enhances the Lethality of Reactive Oxygen Species in Hypoxic Tumor-Targeted Photodynamic Therapy

Miae Won,^{[a]†} Seyoung Koo,^{[a]†} Hao Li,^{[b]†} Jonathan L. Sessler,^{*[c]} Jin Yong Lee,^{*[b]} Amit Sharma,^{*[d]} and Jong Seung Kim^{*[a]}

Abstract: Despite being a clinically approved intervention for cancer, photodynamic therapy (PDT) still suffers from limitations. Prime among these is a therapeutic response that is mostly oxygen dependent. This limits the utility of PDT in treating hypoxic tumors since lower levels of cytotoxic reactive oxygen species (ROS) are generated in regions of low oxygen tension. Glutathione-pi (GST-pi) is a key enzyme that militates against ROS-mediated apoptosis. We report here a new construct, EA-BPS, that contains both a brominated BODIPY photosensitizer (BPS) and an ethacrynic acid (EA) GST-pi inhibitor. Photoirradiation of EA-BPS induces a synergistic antitumor effect that results from the combination of ROS production and GST-pi inhibition. Relative to BPS alone, an enhanced cell-killing effect is seen under hypoxic conditions both *in vitro* and *in vivo*. We conclude that by making better use of the available oxygen in tumor environments, improved therapeutic PDT outcomes should be achievable even under hypoxic conditions.

Photodynamic therapy (PDT) is a clinically established oncologic intervention that relies on the light-mediated activation of photosensitizers (PS) to produce reactive oxygen species (ROS). Many, but not all, PS act to convert molecular oxygen from its triplet ground state to its singlet excited state under conditions of photoirradiation. Singlet oxygen is a recognized ROS that can promote oxidation of key cellular macromolecules and trigger tumor cell death.^[1] PDT enjoys various merits, such as minimal invasiveness, high regioselectivity, low systematic toxicity, and reduced long-term morbidity in certain cancer types.^[2-3] PDT is also being used as an adjunctive treatment after surgical resection where it serves to reduce residual tumor burden.^[4-6] A

considerable body of effort has been devoted to improving the performance of PDT photosensitizers, particularly in the context of cancer therapy.^[7] For example, to avoid the low penetration depth problem associated with the excitation laser,^[8] PS with near-infrared excitation features^[9-10] have been developed, as have a variety of upconverting nanomaterials.^[11-12] Moreover, both chemiluminescence and bioluminescence have been used as excitation light sources.^[13-15] To improve further PDT efficacy with minimal undesired side effects, the targeted delivery of PS to tumor parenchymal cells and subcellular organelle has also been explored.^[16-18] Unfortunately, PDT is an oxygen-dependent therapy and an adequate supply of oxygen at the tumor site is necessary to generate sufficient ROS to induce a robust therapeutic effect. This oxygen dependence limits the utility of PDT in the hypoxic microenvironments of solid tumors.^[19-20] To avoid such limitations, hyperbaric oxygen (O₂) has been used clinically to augment endogenous O₂ supplies in the blood and in tumor tissues.^[21-23] Such approaches are, however, not without risk and can, for instance, lead to O₂-derived toxicity effects in the central nervous system and in the lungs.^[24-25] Various O₂ carriers and *in situ* generators of O₂ have also been explored in an effort to enhance the effectiveness of PDT.^[26-29] However, such strategies can actually lead to the overproduction of ROS under conditions of photoirradiation, thus engendering various side effects.^[30] We suggest that an attractive alternative would involve making the ROS produced during PDT more fatal to malignant cells. This can be accomplished by hampering the endogenous antioxidant-defense systems inherent to cancer cells.

Cancer cells rely on several protective mechanisms to reduce the cellular damage from extracellular oxidants. Inhibiting one or more of these mechanisms could serve to enhance the effective toxicity of the limited ROS produced under conditions of hypoxic PDT. In this study we set out to test the viability of this hypothesis by targeting glutathione S-transferase-pi (GST-pi). GSTs are classified as phase II detoxifying enzymes that play a significant role in homeostasis and intracellular signal transduction.^[31-33] Cytosolic GST-pi participates in various cellular processes, including cellular proliferation, through its non-enzymatic activity.^[34-36] Several reports have highlighted a direct correlation between elevated levels of GST-pi and resistance to anticancer therapies.^[37-38] The combination of PDT with GST-pi gene silencing was used successfully in the case of hepatic carcinoma cells.^[39] Also, the role of GST-pi in modulating the response of cancer cells to PDT has been studied.^[40-42] However, these studies are mostly confined to investigations at the cellular level. The complexity of the *in vivo* environment makes it inherently challenging to translate results from *in vitro* work into more advanced animal studies. Issues of delivery, various protective mechanisms, the presence of potential inhibitory agents, and a variety of other factors can influence the spatial distribution and pharmacokinetics of an administered agent. These factors, individually or collectively can limit the actual PDT performance.

The diuretic drug ethacrynic acid (EA) is widely employed for high blood pressure and proscribed to patients in a severe edematous state.^[43] EA is known to form a covalent Michael

[a] Dr M. Won, Dr S. Koo, Prof J. S. Kim

Department of Chemistry
Korea University
Seoul 02841, Korea
E-mail: jongskim@korea.ac.kr

[b] H. Li, Prof J. Y. Lee

Department of Chemistry
Sungkyunkwan University
Suwon 16419, Korea
E-mail: jinylee@skku.edu

[c] Prof J. L. Sessler

Department of Chemistry
University of Texas at Austin
Austin, Texas 78712-1224, United States
E-mail: sessler@cm.utexas.edu

[d] Dr. A. Sharma

CSIR - Central Scientific Instruments Organisation, Sector-30 C
Chandigarh 160030, India
E-mail: amitorg83@gmail.com

[†] These authors contributed equally to this work
Supporting information and the ORCID identification numbers for the authors of this article can be found under:
<https://doi.org/10.1002/anie.xxxxxxxx>.

RESEARCH ARTICLE

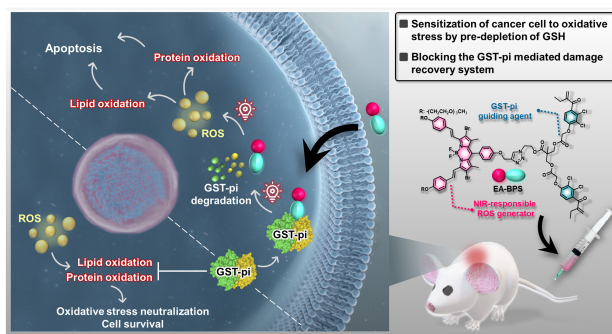


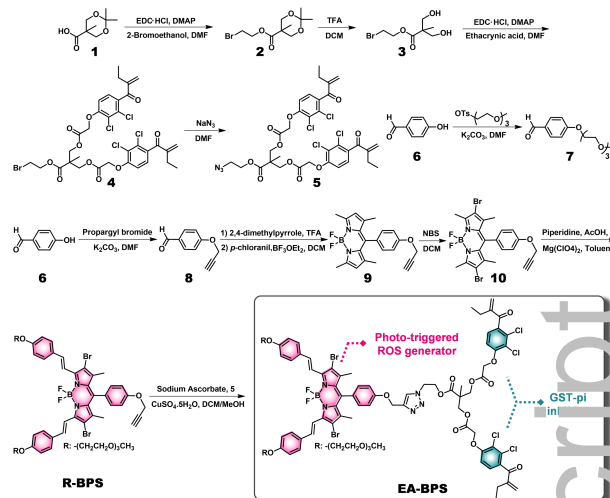
Figure 1. Structure of **EA-BPS** and schematic illustration of the synergistic multi-functional benefit to PDT it is expected to provide including under hypoxic conditions.

addition complex with reduced glutathione (GSH) through the cysteine side chain. This serves to lower the GSH levels and reduce resistance to oxidative stress in cancer cells.^[44] EA has been explored as an anticancer enhancing agent in combination with several chemotherapeutic drugs to improve the treatment outcomes in drug resistance tumors.^[45-48] The EA-GSH conjugate that results from reaction of EA with GSH is relatively non-toxic; however, it has a strong inhibitory effect on the activity of GSTs.^[49] Because cellular damage by ROS is reduced under conditions of elevated GST-pi activity,^[50] we envisaged that GST-pi inhibition in conjunction with PDT would produce a synergistic effect and impart greater lethality to the ROS produced through PDT, even under hypoxic conditions.

Here we show that EA, when covalently linked to a brominated BODIPY-based photosensitizer (BPS) to give conjugate **EA-BPS**, enhances the anticancer performance of PDT under hypoxic conditions. **EA-BPS** was designed to deliver EA to scavenge GSH and simultaneously downregulate GST-pi activity as shown schematically in Figure 1. Our experimental results provide support for the conclusion that EA conjugated to BPS exerts a synergistic effect with PDT both *in vitro* in MDA-MB-231 cells and in a corresponding animal tumor model. *In vitro* mechanistic studies revealed that as compared to various controls, **EA-BPS** significantly reduces the GST-pi activity through a presumed lysosomal degradation pathway and enhances lipid peroxidation. **EA-BPS** also improves PDT-based cytotoxicity under hypoxic conditions and its use regulates the protein expression level of related pro-apoptotic genes. *In vivo* studies, involving the use of a MDA-MB-231 tumor xenograft mouse model, revealed a superior therapeutic effect relative to BPS alone, thus supporting our hypothesis that inhibition of GST-pi activity can lead to PDT-based protocols that exploit relatively effectively the limited oxygen available in tumor microenvironments under hypoxic conditions.

The synthesis of molecular conjugates, **EA-BPS** and **R-BPS** is shown in Scheme 1. Briefly, the diol protected acid intermediate **1** was coupled with 2-bromoethanol in the presence of 1-ethyl-3(3-dimethylaminopropyl)carbodiimide hydrochloride (EDC-HCl) and N,N'-dimethylaminopyridine (DMAP) in dimethylformamide (DMF) to give compound **2**. Subsequent diol deprotection and coupling with ethacrynic acid (EA) in the presence of EDC-HCl, DMAP, and DMF furnished compound **4**. Compound **4** was then treated with sodium azide in DMF to give compound **5**. In parallel, compound **10** was obtained from compound **8** and 2,4-dimethylpyrrole by following a reported procedure.^[16] Intermediate **R-BPS** was then obtained by means of a Knoevenagel condensation between **7** and **10**. Finally, the target compound **EA-BPS** was prepared in good yield via a Cu(I)-mediated alkyne-azo click reaction between intermediates **5** and **R-BPS** in methanol/dichloromethane (10:1). The combined results from nuclear magnetic resonance (NMR) spectroscopy and mass spectrometry (MS) proved consistent with the

structures proposed for all new compounds (Supporting Information, SI, Figure S1-S17).



Scheme 1. Synthesis of **R-BPS** and **EA-BPS**.

We next examined the absorption and emission properties of **R-BPS** and **EA-BPS** in dimethyl sulfoxide (DMSO). An intense absorbance band corresponding to the brominated BODIPY core (BPS) was observed for both **R-BPS** (molar extinction coefficient, $\epsilon = 6.45 \times 10^4 \text{ M}^{-1} \text{ cm}^{-1}$ at 667 nm) and **EA-BPS** ($\epsilon = 7.35 \times 10^4 \text{ M}^{-1} \text{ cm}^{-1}$ at 667 nm) (Figure S18). The fluorescence spectra of **R-BPS** and **EA-BPS** showed an emission peak centered at 698 nm (Figure S18b). The fluorescence emission of both **R-BPS** and **EA-BPS** exhibited hypsochromic shifts (up to 40 nm) with increasing the solvent polarity (p) (tetrahydrofuran, p: 4.0 < acetone, p: 5.1 = methanol, p: 5.1 < acetonitrile, p: 5.8) (Figure S19). We also tested the absorbance and emission properties of **R-BPS** and **EA-BPS** in phosphate buffered saline (PBS) (10 mM, pH 7.4, 1 % Triton X100). Both compounds showed similar absorption (671 nm) and emission (693 nm) characteristics, as determined in organic solvents (Figure S18). However, it is important to appreciate that although emissive, these conjugates incorporate heavy atoms (bromine) in the photosensitizer subunit; this serves to lower the fluorescence quantum yield by promoting intersystem crossing (ISC) to the excited triplet state.^[51]

We next explored whether the enhancement in the ISC rates expected for **R-BPS** and **EA-BPS** would translate into features attractive for PDT. Toward this end 1,3-diphenylisobenzofuran (DPBF) was used as a chemical probe for singlet oxygen (Type 2 ROS) under photosensitizing conditions.^[52] Light irradiation of a mixture of **EA-BPS** and DPBF with 660 nm light showed a sharp decrease in the content of DPBF over 30 min (Figure 2A and 2C). Similar results were obtained for **R-BPS** under otherwise identical experiment conditions, while in the absence of these BPS derivatives, the DPBF content remained unchanged (Figures 2C and S20). The singlet oxygen quantum yields (Φ_{Δ}) for **R-BPS** and **EA-BPS** were determined using a protocol that relies on methylene blue (MB) as the standard (MB: $\Phi_{\Delta} = 0.52$ in DMSO)^[16] giving Φ_{Δ} values of 0.14 and 0.13 for **R-BPS** and **EA-BPS**, respectively (Figure S20).

Separately, 2,7-dichlorodihydrofluorescein diacetate (DCFH-DA) was used as a ROS indicator. DCFH has been reported to behave as a broad ROS sensor (primarily for Type 1 ROS) that reacts with hydroxyl radicals ($\text{HO}\cdot$), peroxy radicals ($\text{ROO}\cdot$), and to a lesser extent superoxide radicals ($\text{O}_2^{\cdot-}$), to give a highly fluorescent daughter product, 2',7'-dichlorofluorescein (DCF).^[53] Both **R-BPS** and **EA-BPS** produced a time-dependent fluorescence enhancement at 523 nm ascribed to DCF upon irradiation (660 nm) for an extended time (Figure 2B and 2D). In contrast, when DCFH-DA was subject to photoirradiation in the

RESEARCH ARTICLE

absence of **R-BPS** or **EA-BPS** the fluorescence increases at 523 nm proved negligible (Figure S21). Moreover, **R-BPS** and **EA-BPS** gave rise to fluorescence spectral changes of dihydrorhodamine 123 (DHR123) and hydroxyl phenyl fluorescein (HPF), which are specific indicators of $O_2^{\cdot-}$ and HO^{\cdot} , respectively, upon light irradiation (Figure S22). Collectively, these results provide support for the contention that under photosensitizing conditions, **R-BPS** and **EA-BPS** are capable of promoting ROS production (in both DMSO and aqueous media) (Figures S20, S21 and S22). We thus considered them worthy of further study.

To identify the active sites and obtain insights into the presumed interactions between GST-pi and **EA-BPS**-(GSH)₂ (a molecule conjugate presumably formed between **EA-BPS** and GSH), docking and molecular dynamics (MD) simulations were performed (Figure 2E and 2F). The binding free energy between GST-pi and **EA-BPS**-(GSH)₂ was calculated to be -65.1 kcal/mol from the MD simulation. Five residues (Chain A: F7, W37 and Y107; Chain B: Y107 and A120) were found to play an important role in the active site, as reflected in the associated deconstructed free energy values of -2.9, -2.4, -4.2, -1.9 and -2.3 kcal/mol, respectively. It is worth noting that Y107 residues are present in the active site, a finding that leads us to infer that **EA-BPS**-(GSH)₂ is interacting with the GST-pi enzyme pocket through both ethacrynic subunits rather than just one (Figure S23).

The stability of agents in biological milieus is an important issue that must be considered in the context of their therapeutic development. Given the fact that **EA-BPS** has an ester functional group, which could lead to low stability in biological media (e.g., be reactive towards esterases), we monitored the time-dependent change in composition of **EA-BPS**, under various solution phase conditions using high performance liquid chromatography (HPLC). As indicated in Figure S24, a peak with retention time of 24.6 min, corresponding to **EA-BPS**, remained unchanged after incubation for 6 h in 10 mM PBS, RPMI 1640, and RPMI 1640 containing 10% FBS. Furthermore, **EA-BPS** was not found to be appreciably hydrolyzed in the presence of esterase while **EA-ester**, the carboxylic ethyl ester form of EA, was quickly hydrolyzed under these same conditions (Scheme S1 and Figure S25). On this basis, we conclude that **EA-BPS** was sufficiently stable so as to allow for further biological studies.

To test whether GST-pi inhibition leads to an improvement in PDT efficacy, the cellular uptake behavior and cytotoxicity of **R-BPS** and **EA-BPS** were investigated. First, the endogenous expression of GST-pi in the human breast cancer cell lines the MDA-MB-231 (GST-pi positive) and MCF7 (GST-pi negative) were confirmed using Western blot analyses. As expected, the GST-pi expression in MDA-MB-231 proved significantly higher than in the MCF7 cell line (cf. Figure S26). Because of their differential expression behavior, these two cell lines were selected for further experiments.

Next, we performed flow cytometry analyses to evaluate the cellular uptake of compounds **R-BPS** and **EA-BPS** in the MDA-MB-231 and MCF7 cell lines. As shown in Figures 3A and S27, **EA-BPS** was taken up more effectively than **R-BPS**. The uptake proved time dependent in both cell lines, with the uptake being greater for the MDA-MB-231 cell line. Considering the structural features of these two compounds, the greater uptake of **EA-BPS** may be due to its more lipophilic character as compared to **R-BPS**. It is known that the lipid bilayer of the cell membrane in cancer cells facilitates the transport of lipophilic agents.^[54] The higher retention **EA-BPS** in the MDA-MB-231 cell line as compared to the MCF7 cell line may also reflect a possible covalent interaction between GSH and the EA subunit and further interactions of the resulting adduct with GST-pi.^[55]

To assess the therapeutic potential of **R-BPS** and **EA-BPS**, cell viability assays were performed without irradiation (test of dark toxicity) using the MCF7 and MDA-MB-231 cancer cell lines. While **R-BPS** was not appreciably cytotoxic up to 50 μ M in both cell lines, the same concentration of **EA-BPS** produced 21% and 42% reduction in the cell viabilities in the MCF7 and MDA-MB-

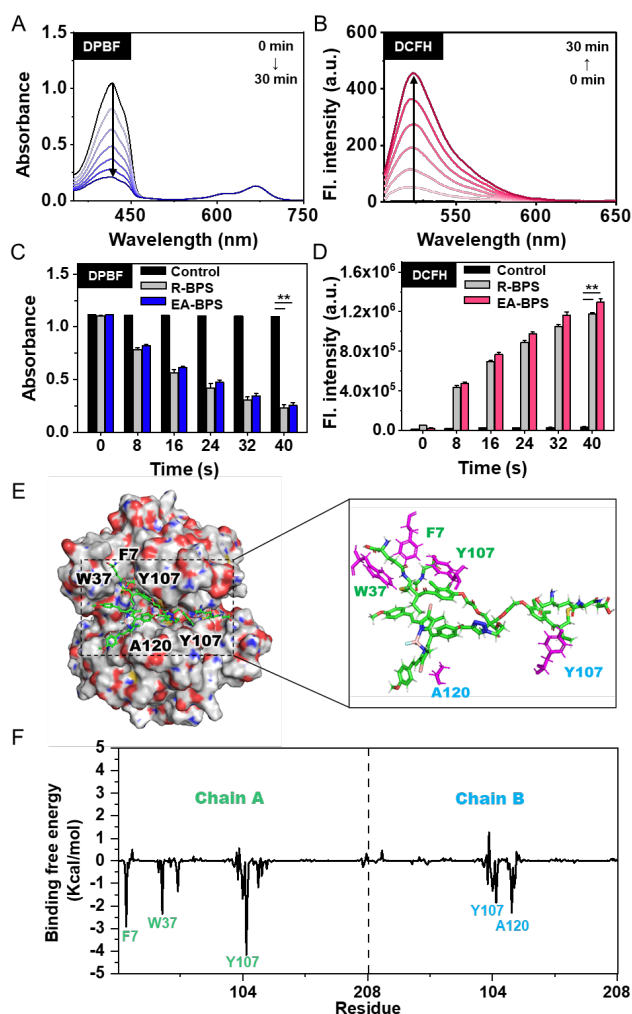


Figure 2. Photodynamic and GST-pi binding properties of **EA-BPS**. Time-dependent (a) absorption spectral changes of DPBF (1O_2 detection) and (b) fluorescence spectral changes of DCFH (ROS detection) upon 660 nm light irradiation (Xe-lamp, slit width 15/1.5 nm) of **EA-BPS**. (c) absorption intensity change of DPBF at 412 nm and (d) fluorescence intensity change of DCFH at 535 nm in the presence of light irradiation (LED lamp, 100 mW/cm²) with **EA-BPS**, **R-BPS** or without BPSs. Binding study of GST-pi and GSH-**EA-BPS**. (e) Calculated GST-pi binding sites. (f) The free energy of binding of each residue of GST-pi with GSH-**EA-BPS**. Bar graph data are presented as the mean, while the error bars indicate the standard deviation from the mean (n = 3). **p<0.001.

231 cell lines, respectively (Figure S28). Upon photoirradiation (660 nm, LED lamp, 100 mW/cm²) for 10 min, the toxicity difference (**R-BPS** vs. **EA-BPS** or MCF7 vs. MDA-MB-231) was enhanced even when 5 μ M concentrations of **R-BPS** and **EA-BPS** were used (Figure S29). **EA-BPS** led to a significant reduction of cell viability in MCF7 cells (31%) and MDA-MB-231 (70%), respectively; however, **R-BPS** produced only a slight decrease in the cell viability in both tested cell lines under similar conditions. These results support our core hypothesis, namely that EA-based blocking of GST-pi activity under conditions of photoirradiation should translate into increased cytotoxicity for cells that are particularly reliant on the GST-pi antioxidant system.

We next investigated the ability of **R-BPS** and **EA-BPS** to produce ROS inside MDA-MB-231 cancer cells under conditions of photoirradiation. The cells were incubated separately with **R-BPS**, **EA-BPS**, and 1% DMSO as a control in the presence of an oxidant-sensitive ROS probe (DCFH-DA, green). Upon photoirradiation (660 nm, 100 mW/cm², 10 min), an intense green

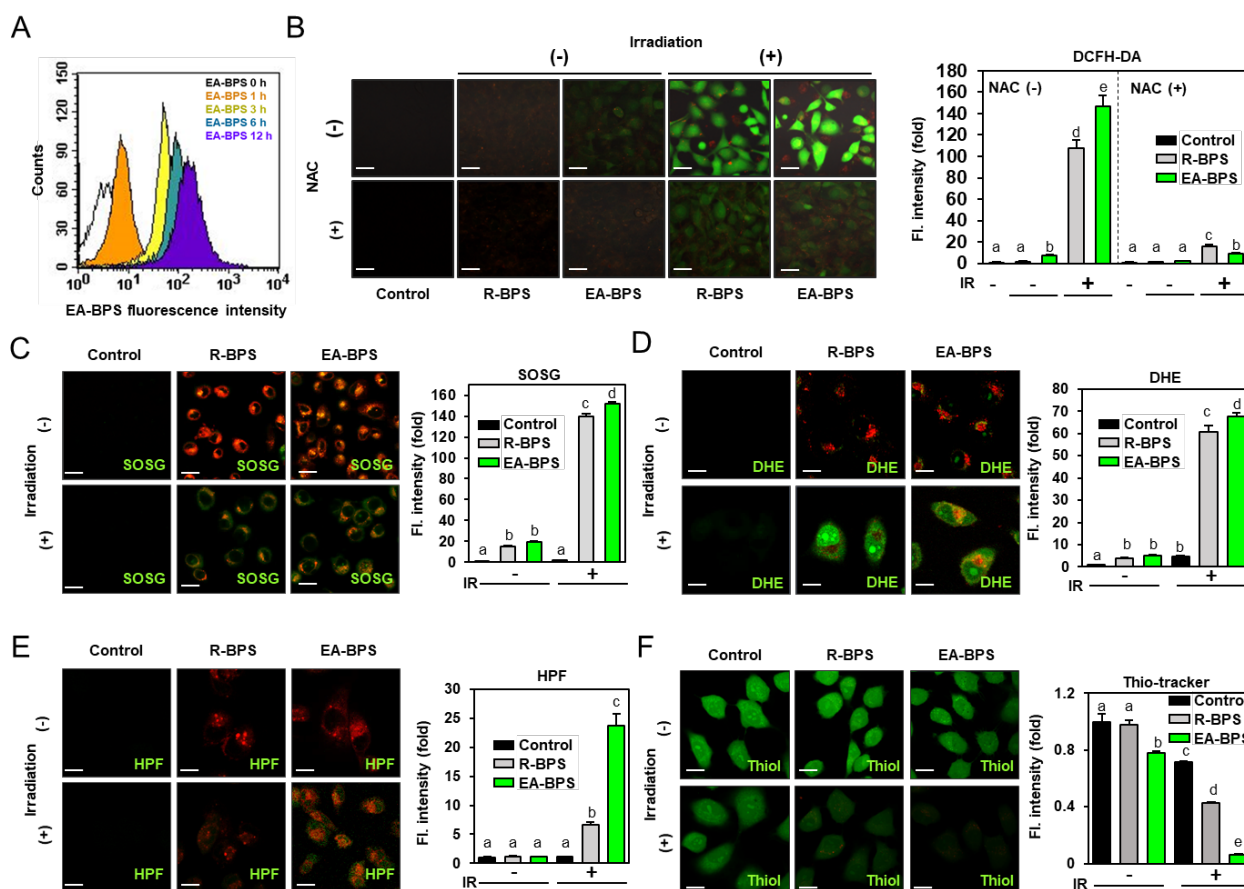


Figure 3. PDT sensitizer potential of EA-BPS. (A) Time-dependent uptake of EA-BPS (5 μM) into MDA-MB-231 cells. (B) The effect of NAC on the ROS burden in R-BPS (5 μM for 12 h), EA-BPS (5 μM for 12 h) and control (1% DMSO for 12 h) challenged cells in the absence and presence of photoirradiation (660 nm LED lamp, 100 mW/cm^2) for 10 min. (C) Singlet oxygen sensor green (SOSG) fluorescence (5 μM for 30 min) in MDA-MB-231 cells incubated with R-BPS (5 μM for 12 h), EA-BPS (5 μM for 12 h) and the absence of a BPS (control, 1% DMSO) in the absence and presence of photoirradiation (660 nm LED lamp, 100 mW/cm^2) for 10 min. (D) Dihydroethidium (DHE) fluorescence (30 μM for 30 min) in MDA-MB-231 cells incubated with R-BPS (5 μM for 12 h), EA-BPS (5 μM for 12 h) and the absence of a BPS (control, 1% DMSO) in the absence and presence of photoirradiation (660 nm LED lamp, 100 mW/cm^2) for 10 min. (E) Hydroxy phenyl fluorescein (HPF) fluorescence (10 μM for 30 min) in MDA-MB-231 cells incubated with R-BPS (5 μM for 12 h), EA-BPS (5 μM for 12 h) and the absence of a BPS (control, 1% DMSO) in the absence and presence of photoirradiation (660 nm LED lamp, 100 mW/cm^2) for 10 min. (F) Intracellular thiol-tracker fluorescence (10 μM for 30 min) in MDA-MB-231 cells incubated with R-BPS (5 μM for 12 h), EA-BPS (5 μM for 12 h) and the absence of a BPS (control, 1% DMSO) in the absence and presence of photoirradiation (660 nm LED lamp, 100 mW/cm^2) for 10 min. Data are presented as the mean, while the error bars indicate the standard deviation from the mean ($n = 9$). Statistical significance was determined using a one-way ANOVA test with a post-hoc Bonferroni test. Different letters signify data that are statistically distinct ($p < 0.05$). Scale bar = 20 μm .

fluorescent signal corresponding to the formation of DCF (the oxidized, fluorescent form of the DCFH-DA probe) was observed from cells incubated with R-BPS and EA-BPS. Quantitative analyses revealed that the fluorescence signal intensity in the cells treated with EA-BPS was greater than that in the corresponding R-BPS group (Figure 3B). In contrast, no fluorescence signal was observed in the control group (1% DMSO). Pre-incubation of the cells with *N*-acetylcysteine (NAC, an effective ROS quencher^[56]) resulted in a diminished green fluorescence when the experiments were carried out under otherwise identical experimental conditions. Based on these results, we conclude that R-BPS and EA-BPS trigger intracellular ROS production upon light activation and that the extent of ROS generation was greater in the case of EA-BPS than R-BPS by ~1.4-fold (Figure 3B).

Typically PDT photosensitizers are classified by whether they promote light-mediated production of ROS through Type I (radical ions formed by the abstraction of an electron/hydrogen atom from a substrate by a photoexcited PS) or Type II (photoexcited PS serving to promote the conversion of triplet ground state

molecular oxygen ($^3\text{O}_2$) to reactive singlet oxygen ($^1\text{O}_2$) mechanisms.^[57-58] In an effort to ascertain which of these limiting mechanisms might be dominant in the case of EA-BPS, we first determined whether $^1\text{O}_2$ was being produced in cells under conditions of photoirradiation. For this analysis, a well-known probe, Singlet Oxygen Sensor Green (SOSG), was used as the indicator.^[59] Illumination of cells incubated with R-BPS and EA-BPS as above were characterized by a high level of green fluorescence ascribed to the SOSG probe (Figure 3C). This finding provides support for the contention that these two PS are able to promote singlet oxygen formation.

To test whether R-BPS and EA-BPS are also able to generate ROS through a Type I mechanism, dihydroethidium (DHE), a widely used fluorescence assay for the detection of intracellular $\text{O}_2^{\cdot-}$,^[60] was used as indicator. As can be seen from an inspection of Figure 3D the fluorescence intensities ascribed to oxidized DHE proved similar for the R-BPS or EA-BPS treated cells, indicating $\text{O}_2^{\cdot-}$ production upon irradiation. Analogous studies were then carried out with hydroxyl phenyl fluorescein (HPF), a chemosensor used for the detection of hydroxyl radical and

RESEARCH ARTICLE

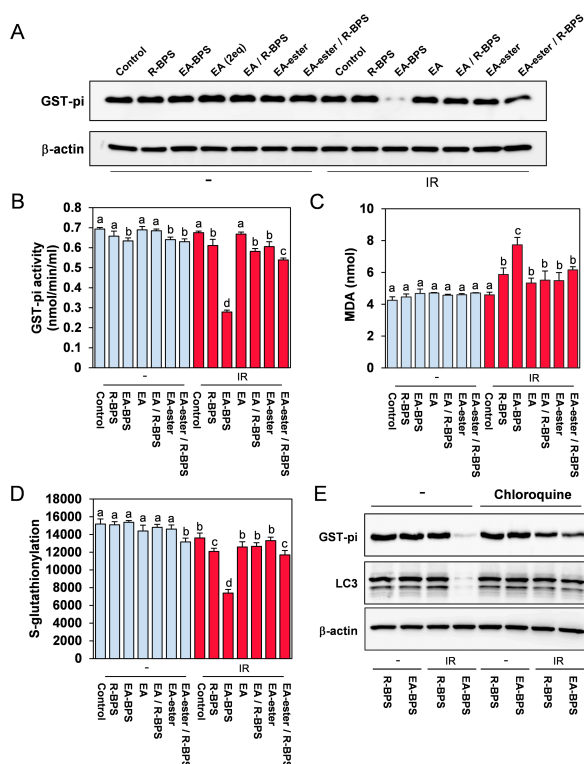


Figure 4. Effect of EA-BPS with and without photoirradiation on lysosomal degradation-dependent way. (A) Western blot analysis of GST-pi expression in MDA-MB-231 cells incubated with **R-BPS** (5 μ M for 12 h), **EA-BPS** (5 μ M for 12 h), EA (2 equiv.), **EA-ester** (2 equiv.) and mixture of **R-BPS** (5 μ M for 12 h) and EA or **EA-ester** (2 equiv. for 12 h) in the absence and presence of photoirradiation (660 nm LED lamp, 100 mW/cm²) for 10 min. (B) GST activity in MDA-MB-231 cells incubated with **R-BPS** (5 μ M for 12 h), **EA-BPS** (5 μ M for 12 h), EA (2 equiv.), **EA-ester** (2 equiv.) and mixture of **R-BPS** (5 μ M for 12 h) and EA or **EA-ester** (2 equiv. for 12 h) in the absence and presence of photoirradiation (660 nm LED lamp, 100 mW/cm²) for 10 min. (C) MDA levels in MDA-MB-231 cells incubated with **R-BPS** (5 μ M for 12 h), **EA-BPS** (5 μ M for 12 h), EA (2 equiv.), **EA-ester** (2 equiv.) and mixture of **R-BPS** (5 μ M for 12 h) and EA or **EA-ester** (2 equiv. for 12 h) in the absence and presence of photoirradiation (660 nm LED lamp, 100 mW/cm²) for 10 min. (D) S-glutathionylation levels in MDA-MB-231 cells incubated with **R-BPS** (5 μ M for 12 h), **EA-BPS** (5 μ M for 12 h), EA (2 equiv.), **EA-ester** (2 equiv.) and mixture of **R-BPS** (5 μ M for 12 h) and EA or **EA-ester** (2 equiv. for 12 h) in the absence and presence of photoirradiation (660 nm LED lamp, 100 mW/cm²) for 10 min. (E) Western blot analysis of GST-pi expression in MDA-MB-231 cells incubated with **R-BPS** and **EA-BPS** in the absence or upon treatment of 10 μ M chloroquine in the absence and presence of photoirradiation (660 nm LED lamp, 100 mW/cm²) for 10 min. The plotted values are the means, while error bars indicate the standard deviation from the mean (n = 6). Statistical significance was determined using a one-way ANOVA test with a post-hoc Bonferroni test. Different letters signify data that are statistically distinct (p < 0.05).

peroxynitrite anions.^[61] It was found that the oxidized HPF signal from the **EA-BPS** treated cells was 3.6-fold higher than in the case of **R-BPS** treated cells (Figure 3E), leading us to conclude that hydroxyl (or peroxynitrite) radicals are being formed. Although, *in vivo* the half-life of the hydroxyl radical is very short (10⁻⁹ s),^[62] due to its high reactivity, it is able to mediate the oxidation of many macromolecules including carbohydrates, lipids, and even amino acids.^[63] Moreover, unlike superoxide, which can be neutralized by superoxide dismutase, hydroxyl radicals are not known to be eliminated via an enzymatic process.^[64] Therefore, the ability to produce hydroxyl (or peroxynitrite) radicals in conjunction with other ROS could explain the greater cytotoxicity seen for **EA-BPS** relative to **R-BPS**.

To obtain further insights into the potential benefits of the EA moiety present in **EA-BPS**, we monitored the levels of GSH expression with and without photoirradiation using a thiol-tracker, Thiol-tracker™ Violet.^[65] In the absence of photoirradiation, a modest (ca. 15%) decrease in the GSH levels in the **EA-BPS** treated cells was observed, while the **R-BPS** treated cells showed nearly the same levels as control (1% DMSO). A very different situation was seen under conditions of photoirradiation. Here, a 7.3-fold reduction in the GSH levels was seen for the **EA-BPS** treated cells compared to the **R-BPS** treated cells (Figure 3F). We conclude that per our design expectations the EA moiety in **EA-BPS** when combined with light serves to reduce the endogenous GSH levels.

Next, to investigate the inhibitory effect of **EA-BPS** on GST-pi, the enzymatic activity and protein levels of GST-pi were measured (Figure 4A and 4B). To evaluate the effect of **EA-BPS** conjugate, control experiments involving co-treatment of **R-BPS** with EA were carried out. Given the presence of a carboxylic acid functional group in EA, which might serve to limit permeability across cellular membrane,^[66-67] the carboxylic ethyl ester form of EA (**EA-ester**) was prepared and tested (Scheme S1). As shown in Figure 4A, photoirradiation of the **EA-BPS** treated group resulted in a remarkable decrease in the GST-pi protein level. In line with these results, **EA-BPS** when subject to photoirradiation, served to reduce the GST-pi activity by 58% (Figure 4B). In contrast, **R-BPS** and mixture of **R-BPS** and EA or **EA-ester** only reduced the GST-pi activity by 5-20% under similar conditions (Figure 4B).

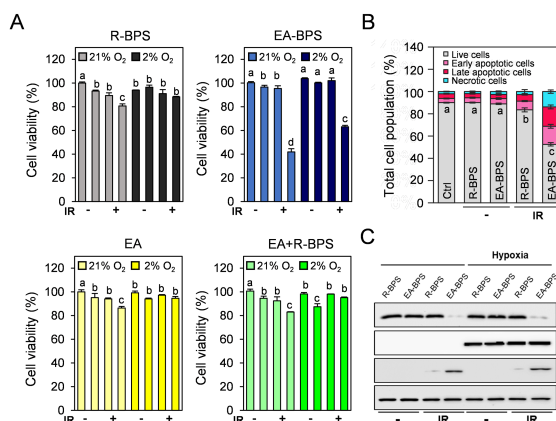


Figure 5. Hypoxia induced apoptotic cell death by **EA-BPS**. (A) Cell viability of MDA-MB-231 cells incubated with **R-BPS**, **EA-BPS**, mixture of **R-BPS** and EA or EA under normoxia (21% O₂) and hypoxia (2% O₂) in the absence and presence of photoirradiation (660 nm LED lamp, 100 mW/cm²) for 10 min. (B) Cell population graph of MDA-MB-231 treated with **R-BPS** and **EA-BPS** for 12 h in the absence and presence of photoirradiation (660 nm LED lamp, 100 mW/cm²) for 10 min by flow cytometry. (C) Apoptotic cell death assay of **R-BPS** and **EA-BPS** under 2% O₂ (hypoxia) as determined by western blot analysis. Values are the mean, while error bars indicate the standard deviation from the mean (n = 6). Statistical significance was determined using a one-way ANOVA test with a post-hoc Bonferroni test. Different letters signify data that are statistically distinct (p < 0.05).

The effect of this reduction on downstream events was then studied. It was previously reported that GST-pi facilitates the detoxification and removal of lipid peroxides by activation of peroxiredoxin VI (Prdx6), which has peroxidase activity.^[68] Appreciating this, malondialdehyde (MDA), one of the final products of lipid peroxidation^[69] was measured in the presence of **R-BPS** and **EA-BPS** with and without photoirradiation using a commercially available lipid peroxidation MDA assay kit (Figure 4C). Consistent with its effect on GST-pi activity, **EA-BPS** was found to promote an increase in the MDA levels as compared to **R-BPS** and mixtures of **R-BPS** and EA or **EA-ester**.

RESEARCH ARTICLE

GST-pi has also been reported to promote the S-glutathionylation of damaged proteins.^[70] The extent of protein S-glutathionylated was thus also monitored in the presence of **R-BPS**, **EA-BPS** and mixtures of **R-BPS** and EA or **EA-ester** under conditions of photoirradiation. In accord with what would be expected for a system that reduces GST-pi activity, **EA-BPS** was found to lower the S-glutathionylated protein levels by roughly 50%, whereas the reduction seen in the case of **R-BPS** and mixture of **R-BPS** and EA or **EA-ester** proved far more modest (Figure 4D). These findings are consistent with a mode of action for **EA-BPS** under conditions of photoirradiation that benefits from the inhibition of innate detoxification processes normally exploited by cancer cells.

To explore the mechanisms of GST-pi degradation mediated by **EA-BPS** under conditions of photoirradiation, we pre-treated MDA-MB-231 cells with 3 μ M of chloroquine (CQ) (a lysosomal inhibitor).^[71] It was observed that LC3 (an autophagy marker) protein expression was diminished in a statistically significant manner under conditions of photoirradiation in the presence of **EA-BPS** (Figure 4E). CQ treatment also induced GST-pi expression. Collectively, these results provide support for the notion that **EA-BPS** promotes a lysosomal degradation pathway and inhibits GST-pi activity (Figure 4E). Overlap between the red fluorescence ascribed to the BPS subunit and the green fluorescence due to the LysoTracker® and MitoTracker® probes revealed that after photoirradiation **EA-BPS** is not only localized in lysosomes but also in the mitochondria (Figure S30).

To assess further the photo-induced toxicity of **EA-BPS** in tumor micro-environments, MDA-MB-231 cells were pre-incubated under normoxic and hypoxic conditions. The cells were subsequently treated with **R-BPS**, **EA-BPS**, EA only, and EA in conjunction with **R-BPS** with or without photoirradiation. As can be seen from an inspection of Figure 5A, little appreciable toxicity was seen when MDA-MB-231 cells treated with **R-BPS**, EA only, or EA in combination with **R-BPS** were subject to photoirradiation under hypoxic conditions. In contrast, remarkable cytotoxicity was seen in the case of the cells treated with **EA-BPS** and then subject to photoirradiation under both normoxic (21% O₂) and hypoxic conditions (2% O₂).

Cell death signaling mechanisms for the cells treated with **EA-BPS** under conditions of photoirradiation were investigated by means of annexin V and western blot assays (Figure 5B and 5C). An annexin-V/propidium iodide (PI) staining assay revealed that **EA-BPS** under conditions of photoirradiation increased the population of annexin V-positive apoptotic cells (to 50%) compared to the other tested groups (Figures 5B and S31: $\leq 8\%$). An increase in cleaved caspase-3 levels was also seen upon photoirradiation under hypoxic conditions. This latter finding supports the conclusion that treatment of MDA-MB-231 cells with **EA-BPS** leads to reduced expression of the GST-pi protein (Figure 5C) and that the observed improvements in therapeutic efficacy can be ascribed to a hampering of the GST-pi mediated endogenous antioxidant-defense system.

MDA-MB-231 tumor xenograft-bearing mice were used to test the efficacy of **EA-BPS** as a PDT photosensitizer in a model hypoxic tumor microenvironment. In these studies **EA-BPS** (5 mg/kg in PBS containing 5% DMSO) was administered intravenously via tail vein injection. A readily discernible fluorescence signal was observed at the tumor site up to 48 h post administration (Figures 6A and S32). *Ex vivo* imaging of dissected organs collected from the mice treated with **EA-BPS** (48 h post-administration) served to confirm that the observed fluorescence signal corresponded to the tumor site. Little fluorescence was seen for the other organs (liver, heart, kidney, spleen, testis, and lung) (Figures 6B and S33). Mice treated with **EA-BPS** (5 mg/kg in PBS containing 5% DMSO) and subject to photoirradiation (2 W/cm², 10 min, once a week for 4 weeks) at the tumor regions showed a statistically significant reduction in tumor growth and volumes (Figure 6C). Furthermore, no significant changes in the animal body weights was observed during the course of

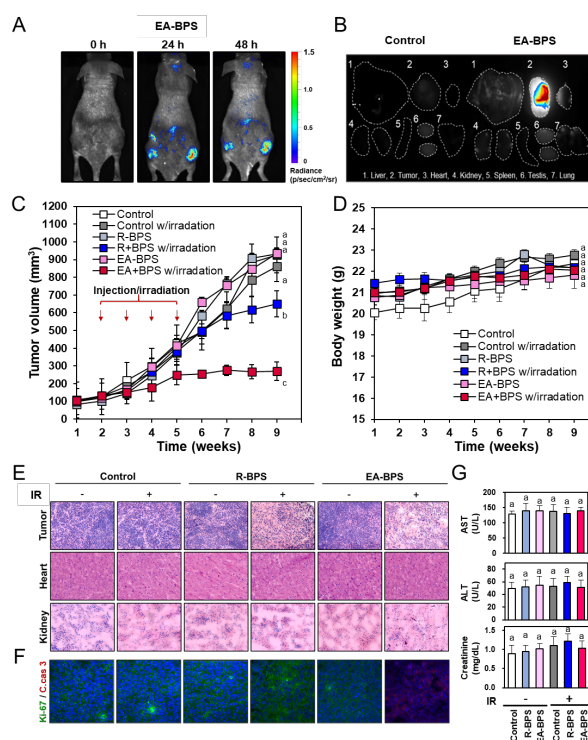


Figure 6. In vivo photodynamic effects and tumor regression seen in MDA-MB-231 xenograft mouse models. (A) In vivo biophy fluorescence images of an MDA-MB-231 xenograft mouse 1, 24, and 48 h after intravenous tail-vein injection of a single dose of 5 mg/kg **EA-BPS** (excitation at 660 nm; emission at 700 nm). (B) Ex vivo images of excised tumors and organs recorded 48 h after injecting single dose of 5 mg/kg **EA-BPS** or vehicle alone (PBS containing 5% DMSO). (C) In vivo tumor volumes ($1/2 \times \text{length} \times \text{width}^2$) determined in MDA-MB-231 xenograft mice treated 6 h after injecting with 5 mg/kg **R-BPS**, **EA-BPS** or vehicle alone for 4 weeks (once a week) in the absence and presence of photoirradiation (660 nm, 2 W/cm², 10 min). (D) Body weight of mice recorded during the treatment regime. (E) H&E staining of representative tissue slices of the different treatment groups at the study endpoint. (F) Immunohistochemistry (IHC) of representative tumor tissue slices taken from the different treatment groups. (G) Blood serum AST, ALT and creatinine activity levels, as determined using a colorimetric assay. The values are the means, while the error bars indicate s.e.m. (standard error of the mean). Panels c, d, g: n = 5 mice per group. Statistical significance was determined using a one-way ANOVA test with a post-hoc Bonferroni test. Different letters signify data that are statistically different ($p < 0.05$). The symbols + and - are used to denote the presence and absence of photoirradiation.

treatment; this was true for both the **EA-BPS** test groups and the various controls (Figure 6D).

The *in vivo* phototherapeutic effects were further confirmed by examining tumor and tissue sections from animals in the test and control groups through hematoxylin & eosin (H&E) staining and immunohistochemistry (IHC) assays. The H&E-stained tumor sections taken from the xenograft mice treated with **EA-BPS** and subject to photoirradiation showed characteristic apoptotic cells, while no such effect was seen in other groups (Figure 6E). Cleaved caspase-3 (red) levels were greater in the mice treated with **EA-BPS** and subject to photoirradiation. Also, the Ki-67 expression levels (green) were downregulated, indicating a dramatic reduction in cell proliferation in the **EA-BPS** treated mice (Figures 6F and S34). No such effects were observed in the tumor sections taken from animals treated with **R-BPS** or in the control group (5% DMSO in PBS). Further, no apparent clinical side-effects were seen in the test and control groups during the experiments or at their endpoint. Finally, the AST (aspartate

RESEARCH ARTICLE

transaminase), ALT (alanine aminotransferase) and creatinine activity levels were within the normal range (Figure 6G).^[72] Collectively, these results were taken as evidence that under the conditions of study, **EA-BPS** is biocompatible and is likely to benefit from by an acceptable safety profile.

In conclusion, one of the major limitations of PDT, and one with severe clinical repercussions, is the fact that the endogenous antioxidant system of mammalian cells serves to mitigate the effects of ROS generation. In this study we have shown that an EA-bearing photosensitizer conjugate (**EA-BPS**) that *inter alia* reduces the effectiveness of GST-pi enhances the cytotoxicity of PDT-derived ROS in cancer cells under both normoxic and hypoxic conditions. In particular, synergistic therapeutic effects were observed in a GST-pi overexpressing cancer cell line both *in vitro* and *in vivo*. The enhanced effectiveness seen for **EA-BPS** is ascribed to an ability to reduce the innate ROS detoxification processes exploited by cancer cells, which makes hypoxic tumors relatively less susceptible to PDT. Based on the results presented here, we suggest that conjugates such as **EA-BPS** could prove useful in harnessing the limited oxygen levels present in hypoxic tumors thereby improving the performance of PDT. More broadly, the present work serves to underscore how new rational design approaches may be used to overcome the inherent limitations of PDT.

Acknowledgements

This work was supported by the National Research Foundation of Korea (NRF) funded by the Ministry of Science and ICT (CRI project no. 2018R1A3B1052702 and NRF-2019M3E5D1A01068998, J.S.K.) and funded by the Ministry of Education (Basic Science Research Program 2020R1A6A3A01100551, M.W. and 2020R1A6A3A01100558, S.K.). A.S. thanks the Department of Biotechnology, New Delhi, for a prestigious Ramalingaswami Fellowship 2019 (Grant No. BT/RLF/Re-entry/59/2018). The Robert A. Welch Foundation (F-0018 to J.L.S.) is also acknowledged.

Conflict of interest

The authors declare no conflict of interest.

Keywords: Ethacrynic acid • Photodynamic therapy • Glutathione S-transferase -pi • Reactive oxygen species • BODIPY photosensitizer • Hypoxia

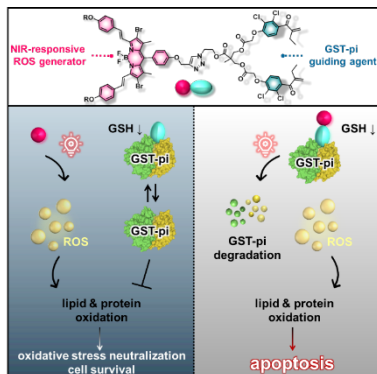
- [1] N. L. Oleinick, R. L. Morris, T. Belichenko, *Photochem. Photobiol. Sci.* **2002**, *1*, 1-21.
- [2] P. Agostinis, K. Berg, K. A. Cengel, T. H. Foster, A. W. Girotti, S. O. Gollnick, S. M. Hahn, M. R. Hamblin, A. Juzeniene, D. Kessel, M. Korbelik, J. Moan, P. Mroz, D. Nowis, J. Piette, B. C. Wilson, J. Golab, *Ca-Cancer J. Clin.* **2011**, *61*, 250-281.
- [3] W. P. Fan, N. Lu, C. Xu, Y. J. Liu, J. Lin, S. Wang, Z. Y. Shen, Z. Yang, J. L. Qu, T. F. Wang, S. P. Chen, P. Huang, X. Y. Chen, *ACS Nano* **2017**, *11*, 5864-5872.
- [4] P. Baas, L. Murrer, F. A. N. Zoetmulder, F. A. Stewart, H. B. Ris, N. vanZandwijk, J. L. Peterse, E. J. T. Rutgers, *Br. J. Cancer* **1997**, *76*, 819-826.
- [5] L. Caesar, T. E. M. van Doeveren, I. B. Tan, A. Dilci, R. L. P. van Veen, B. Karakullukcu, *Photodiagn. Photodyn. Ther.* **2015**, *12*, 414-421.
- [6] T. E. M. van Doeveren, M. B. Karakullukcu, R. L. P. van Veen, M. Lopez-Yurda, W. H. Schreuder, I. B. Tan, *Laryngoscope* **2018**, *128*, 657-663.
- [7] W. P. Fan, P. Huang, X. Y. Chen, *Chem. Soc. Rev.* **2016**, *45*, 6488-6519.
- [8] R. Weissleder, *Nat. Biotechnol.* **2001**, *19*, 316-317.
- [9] J. Dai, Y. H. Li, Z. Long, R. M. Jiang, Z. Y. Zhuang, Z. M. Wang, Z. J. Zhao, X. D. Lou, F. Xia, B. Z. Tang, *ACS Nano* **2020**, *14*, 854-866.
- [10] K. R. Deng, C. X. Li, S. S. Huang, B. G. Xing, D. Y. Jin, Q. G. Zeng, Z. Y. Hou, J. Lin, *Small* **2017**, *13*, 1702299.
- [11] M. R. Hamblin, *Dalton Trans.* **2018**, *47*, 8571-8580.
- [12] S. S. Lucky, K. C. Soo, Y. Zhang, *Chem. Rev.* **2015**, *115*, 1990-2042.
- [13] C. M. Magalhaes, J. C. G. E. da Silva, L. P. da Silva, *Chemphyschem* **2016**, *17*, 2286-2294.
- [14] D. Mao, W. B. Wu, S. L. Ji, C. Chen, F. Hu, D. L. Kong, D. Ding, B. Liu, *Chem* **2017**, *3*, 991-1007.
- [15] Y. R. Kim, S. Kim, J. W. Choi, S. Y. Choi, S. H. Lee, H. Kim, S. K. Hahn, G. Y. Koh, S. H. Yun, *Theranostics* **2015**, *5*, 805-817.
- [16] H. S. Jung, J. Han, H. Shi, S. Koo, H. Singh, H. J. Kim, J. L. Sessler, J. Y. Lee, J. H. Kim, J. S. Kim, *J. Am. Chem. Soc.* **2017**, *139*, 7595-7602.
- [17] M. L. Li, J. Xia, R. S. Tian, J. Y. Wang, J. L. Fan, J. J. Du, S. Long, X. Z. Song, J. W. Foley, X. J. Peng, *J. Am. Chem. Soc.* **2018**, *140*, 14851-14859.
- [18] D. D. Zhang, L. W. Wen, R. Huang, H. H. Wang, X. L. Hu, D. Xing, *Biomaterials* **2018**, *153*, 14-26.
- [19] J. M. Brown, W. R. William, *Nat. Rev. Cancer* **2004**, *4*, 437-447.
- [20] A. Sharma, J. F. Arambula, S. Koo, R. Kumar, H. Singh, J. L. Sessler, J. S. Kim, *Chem. Soc. Rev.* **2019**, *48*, 771-813.
- [21] K. Stepien, R. P. Ostrowski, E. Matyja, *Med. Oncol.* **2016**, *33*.
- [22] M. Hockel, P. Vaupel, *J. Natl. Cancer Inst.* **2001**, *93*, 266-276.
- [23] Z. H. Lu, J. W. Ma, B. Liu, C. G. Dai, T. Xie, X. Y. Ma, M. Li, J. Dong, Q. Lan, Q. Huang, *Cancer Med.* **2016**, *5*, 3147-3155.
- [24] Y. L. Chen, Y. N. Zhang, Z. Z. Wang, W. G. Xu, R. P. Li, J. D. Zhang, *Brain Res.* **2016**, *1635*, 180-189.
- [25] A. Hadanny, T. Zubari, L. Tamir-Adler, Y. Bechor, G. Fishlev, E. Lang, N. Polak, J. Bergan, M. Friedman, S. Efrati, *BMC Pulm. Med.* **2019**, *19*, 148.
- [26] Y. H. Cheng, H. Cheng, C. X. Jiang, X. F. Qiu, K. K. Wang, W. Huan, A. Yuan, J. H. Wu, Y. Q. Hu, *Nat. Commun.* **2015**, *6*, 8785.
- [27] M. Yu, X. L. Xu, Y. J. Cai, L. Y. Zou, X. T. Shuai, *Biomaterials* **2018**, *175*, 61-71.
- [28] C. C. Huang, W. T. Chia, M. F. Chung, K. J. Lin, C. W. Hsiao, C. Jin, W. H. Lim, C. C. Chen, H. W. Sung, *J. Am. Chem. Soc.* **2016**, *138*, 5222-5225.
- [29] D. D. Wang, H. H. Wu, W. Q. Lim, S. Z. F. Phua, P. P. Xu, Q. W. Chen, Z. Guo, Y. L. Zhao, *Adv. Mater.* **2019**, *31*, e1901893.
- [30] R. R. Allison, *Future Oncol.* **2014**, *10*, 123-142.
- [31] E. Laborde, *Cell Death Differ.* **2010**, *17*, 1373-1380.
- [32] J. D. Hayes, J. U. Flanagan, I. R. Jowsey, *Annu. Rev. Pharmacol. Toxicol.* **2005**, *45*, 51-88.
- [33] B. Mannervik, P. G. Board, J. D. Hayes, I. Listowsky, W. R. Pearson, *Methods Enzymol.* **2005**, *401*, 1-8.
- [34] V. Adler, Z. M. Yin, S. Y. Fuchs, M. Benezra, L. Rosario, K. D. Tew, M. R. Pincus, M. Sardana, C. J. Henderson, C. R. Wolf, R. J. Davis, Z. Ronai, *EMBO J.* **1999**, *18*, 1321-1334.
- [35] D. Chen, J. J. Liu, B. Rui, M. Gao, N. W. Zhao, S. Sun, A. J. Bi, T. T. Yang, Y. T. Guo, Z. M. Yin, L. Luo, *Biochim. Biophys. Acta, Mol. Cell Res.* **2014**, *1843*, 454-463.
- [36] K. D. Tew, Y. Manevich, C. Grek, Y. Xiong, J. Uys, D. M. Townsend, *Free Radical Bio. Med.* **2011**, *51*, 299-313.
- [37] K. D. Tew, *Cancer Res.* **2016**, *76*, 7-9.
- [38] N. Allocati, M. Masulli, C. Di Ilio, L. Federici, *Oncogenesis* **2018**, *7*, 8.
- [39] V. Rapozzi, C. Lombardo, S. Cogoi, C. Comuzzi, L. Xodo, *ChemMedChem* **2008**, *3*, 565-568.
- [40] T. A. Theodossiou, C. E. Olsen, M. Jonsson, A. Kubin, J. S. Hotherhall, K. Berg, *Redox Biol.* **2017**, *12*, 191-197.
- [41] M. J. Dabrowski, D. Maeda, J. Zebala, W. D. Lu, S. Mahajan, T. J. Kavanagh, W. M. Atkins, *Arch. Biochem. Biophys.* **2006**, *449*, 94-103.
- [42] L. Larue, B. Myrzakhmetov, A. Ben-Mihoub, A. Moussaron, N. Thomas, P. Arnoux, F. Baros, R. Vanderesse, S. Acherar, C. Frochot, *Pharmaceuticals* **2019**, *12*, 163.
- [43] G. C. Wall, D. Bigner, S. Craig, D. Moines, *Arch. Intern. Med.* **2003**, *163*, 116-117.

RESEARCH ARTICLE

- [44] S. Awasthi, S. K. Srivastava, F. Ahmad, H. Ahmad, G. A. S. Ansari, *Biochim. Biophys. Acta, Protein Struct. Mol. Enzymol.* **1993**, *1164*, 173-178.
- [45] T. Rhodes, P. R. Twentyman, *Br. J. Cancer* **1992**, *65*, 684-690.
- [46] W. H. Ang, I. Khalaila, C. S. Allardyce, L. Juillerat-Jeanneret, P. J. Dyson, *J. Am. Chem. Soc.* **2005**, *127*, 1382-1383.
- [47] B. Liu, X. P. Huang, Y. L. Hu, T. T. Chen, B. Y. Peng, N. N. Gao, Z. C. Jin, T. L. Jia, N. Zhang, Z. L. Wang, G. Y. Jin, *Oncotarget* **2016**, *7*, 58038-58050.
- [48] J. Hansson, K. Berhane, V. M. Castro, U. Jungnelius, B. Mannervik, U. Ringborg, *Cancer Res.* **1991**, *51*, 94-98.
- [49] J. H. T. M. Ploemen, B. Vanommen, J. J. P. Bogaards, P. J. Vanbladeren, *Xenobiotica* **1993**, *23*, 913-923.
- [50] N. Fujitani, A. Yoneda, M. Takahashi, A. Takasawa, T. Aoyama, T. Miyazaki, *Sci. Rep.* **2019**, *9*, 14764.
- [51] Y. P. Rey, D. G. Abradelo, N. Santschi, C. A. Strassert, R. Gilmour, *Eur. J. Org. Chem.* **2017**, *2017*, 2170-2178.
- [52] I. B. C. Matheson, J. Lee, B. S. Yamanashi, M. L. Wolbarsht, *J. Am. Chem. Soc.* **1974**, *96*, 3343-3348.
- [53] B. Kalyanaraman, V. Darley-Usmar, K. J. A. Davies, P. A. Dennerly, H. J. Forman, M. B. Grisham, G. E. Mann, K. Moore, L. J. Roberts, H. Ischiropoulos, *Free Radical Bio. Med.* **2012**, *52*, 1-6.
- [54] C. Peetla, S. Vijayaraghavalu, V. Labhasetwar, *Adv. Drug Delivery Rev.* **2013**, *65*, 1686-1698.
- [55] J. H. Ploemen, A. Van Schanke, B. Van Ommen, P. J. Van Bladeren, *Cancer Res.* **1994**, *54*, 915-919.
- [56] S. Y. Sun, *Cancer Biol. Ther.* **2010**, *9*, 109-110.
- [57] M. R. Hamblin, P. Mroz, *Advances in Photodynamic Therapy: Basic, Translational and Clinical (Engineering in Medicine & Biology)*, 1 ed., Artech House, **2008**.
- [58] X. S. Li, N. Kwon, T. Guo, Z. Liu, J. Yoon, *Angew. Chem. Int. Ed.* **2018**, *57*, 11522-11531.
- [59] S. Kim, M. Fujitsuka, T. Majima, *J. Phys. Chem. B* **2013**, *117*, 13985-13992.
- [60] J. Zielonka, J. Vasquez-Vivar, B. Kalyanaraman, *Nat. Protoc.* **2008**, *3*, 8-21.
- [61] H. Ding, H. Yu, Y. Dong, R. Tian, G. Huang, D. A. Boothman, B. D. Sumer, J. Gao, *J. Control. Release* **2011**, *156*, 276-280.
- [62] H. Sies, *Eur. J. Biochem.* **1993**, *215*, 213-219.
- [63] R. J. Reiter, R. C. Carneiro, C. S. Oh, *Horm. Metab. Res.* **1997**, *29*, 363-372.
- [64] R. J. Reiter, D. Melchiorri, E. Sewerynek, B. Poeggeler, L. Barlow-Walden, J. Chuang, G. G. Ortiz, D. Acuna-Castroviejo, *J. Pineal. Res.* **1995**, *18*, 1-11.
- [65] A. Neuwelt, J. Wu, N. Knap, M. Losin, E. Neuwelt, M. Pagel, S. Warmann, J. Fuchs, P. Czauderna, M. Wozniak, *Neoplasia* **2009**, *11*, 1003-1011.
- [66] P. Lassalas, B. Gay, C. Lasfargeas, M. J. James, V. Tran, K. G. Vijayendran, K. R. Brunden, M. C. Kozlowski, C. J. Thomas, A. B. Smith, D. M. Huryn, C. Ballatore, *J. Med. Chem.* **2016**, *59*, 3183-3203.
- [67] R. Wang, C. Li, D. Song, G. Zhao, L. Zhao, Y. Jing, *Cancer Res.* **2007**, *67*, 7856-7864.
- [68] Y. Manevich, S. I. Feinstein, A. B. Fisher, *Proc. Natl. Acad. Sci. U. S. A.* **2004**, *101*, 3780-3785.
- [69] H. Esterbauer, R. J. Schaur, H. Zollner, *Free Radical Bio. Med.* **1991**, *11*, 81-128.
- [70] I. Dalle-Donne, R. Rossi, G. Colombo, D. Giustarini, A. Milzani, *Trends Biochem. Sci.* **2009**, *34*, 85-96.
- [71] C. A. Homewood, D. C. Warhurst, W. Peters, V. C. Baggaley, *Nature* **1972**, *235*, 50-52.
- [72] Yuh-Pyng Sher, M.-C. Hung, *Bio-Protoc.* **2013**, *3*, e931.

RESEARCH ARTICLE

Entry for the Table of Contents



A molecular construct (**EA-BPS**) has been prepared that overcomes hypoxia-mediated resistance in pre-clinical PDT therapy models.

M. Won, S. Koo, H. Li, J. L. Sessler,* J. Y. Lee,* A. Sharma,* J. S. Kim*

Page No. – Page No.

Enhancing the Lethality of Reactive Oxygen Species in Photodynamic Therapy Targeting Hypoxic Tumors